Effect of a Herringbone Mesostructure on the Electromechanical Properties of Piezofiber Composites for Energy Harvesting Applications

R. Avazmohammadi[1] and R. Hashemi[2,*]

[1]*Institute for Computational Engineering and Sciences, University of Texas at Austin, Austin, Texas 78712, USA*

[2]*Department of Mechanical and Aerospace Engineering, Rutgers University, New Brunswick, New Jersey 08903, USA*

(Received 7 July 2016; revised manuscript received 16 November 2016; published 13 February 2017)

Piezoelectric materials are often used in energy harvesting devices that convert the waste mechanical energy into effective electrical energy. Polymer-based piezoelectric composites appear to be promising candidates for use in these devices, as they offer a number of advantages, such as sufficient flexibility and environmental compatibility. However, a major drawback associated with these composites may be that their effective electromechanical properties are usually weaker than those of the piezoelectric constituents used in them. In this paper, we propose a class of polymeric-based piezoelectric composites with a laminated mesostructure that offer improved electromechanical properties over unidirectional piezofiber composites and can even possess stronger electromechanical properties than their piezoelectric constituents for certain modes of operation. We present examples of enhanced properties of these composites including effective piezoelectric charge and voltage coefficients, as well as effective electromechanical coupling factors for two-dimensional operation modes. We conduct an optimization to identify the optimal microstructure for the highest values of the coupling coefficients within this class of composites. Our findings demonstrate the potential in designing piezoelectric composites with a hierarchical structure to achieve significantly amplified electromechanical properties for energy harvesting applications.

DOI: 10.1103/PhysRevApplied.7.024017

I. INTRODUCTION

Piezoelectric materials can convert mechanical forces into electrical energy (known as the direct piezoelectric effect), and, because of this characteristic, they have found extensive applications in smart devices, such as sensors, transducers, and microgenerators. For example, piezoelectric materials have received considerable attention for enabling self-powered electronic devices that can scavenge ambient mechanical energy and convert it to usable electricity. For instance, with recent advances in microelectronics, there is increasing interest in producing smart portable systems that can harvest abundant dissipating energy from a variety of body movements to replace batteries in low-power-application devices, such as health monitors [1–4].

A widely used piezoelectric material for energy harvesting applications is lead zirconate titanate (PZT). Although PZT offers excellent piezoelectric properties for energy harvesting purposes, its weight, high brittleness, and inflexibility pose some limitations for single-phase application of this material in self-powered systems [2,5]. By contrast, fiber-based piezoelectric composites that consist of an inactive polymeric matrix and a distribution of aligned cylindrical PZT fibers can offer lighter, more flexible, and more mechanically robust and environmentally compatible alternatives to single-phase PZT materials [2,6–8]. On the other hand, a key drawback of using piezoelectric composites over single-phase piezoelectric ceramics may be that the overall piezoelectric properties and harvesting performance of the composites could be compromised [9]. Piezoelectric charge and voltage coefficients (denoted by d and g, respectively) are two important parameters for characterizing the energy harvesting capabilities of a piezoelectric material. Several studies on piezoelectric fiber composites have shown that incorporations of small to moderate fractions of ceramic PZT as continuous parallel fibers in a polymeric matrix lead to composites with noticeably weaker effective charge coefficients than those of the fibers, although they will possess stronger effective voltage coefficients [7,10,11]. Moreover, the electromechanical coupling factors (denoted by k) of these composites that involve both the d and g coefficients decrease compared to those of the constituent piezoelectric fibers. Therefore, the amount of power generated by piezoelectric composite materials still needs to be improved to be comparable with those of single-phase piezoelectric materials to meet the power requirement for the regular operations of many portable electronics in real-world applications.

It is well known that the details of the microstructure of piezoelectric composites have a significant influence on the

*Corresponding author.
rh416@scarletmail.rutgers.edu

effective electromechanical behavior of these composites due to the large contrast between the piezoelectric properties of the fibers and the inactive matrix [5,6,11–13]. Accordingly, a key mission in producing piezoelectric fiber composites is to design the microstructural characteristics of the composites in such a manner that maximizes the desirable piezoelectric coefficients for producing higher power output. For example, Dunn and Taya [11] studied the effect of fiber shape on the effective properties of piezoelectric composites consisting of a polymeric matrix and aligned, long cylindrical piezoelectric fibers of an elliptical cross section. Using the Mori-Tanaka homogenization scheme, they showed that increasing the (in-plane) aspect ratio of the fibers leads to an improvement in piezoelectric performance for the operation mode associated with the elongated direction of the fibers, and the performance continues to improve as fibers become more elongated. However, the effective charge coefficients of the composite always remain less than those of piezoelectric fibers—even in the extreme case of infinity—elongated fibers in which fibers approach a plate (or layer) shape. For future reference, we note that the latter composites that consist of two alternating layers are referred to as rank-1 laminated composites. If each layer is composed of other alternating layers, the composite will be referred to as rank 2, and so on.

In this work, we propose a class of *hierarchical* laminated piezoelectric composites (LPCs) that offer significantly improved effective electromechanical properties over the corresponding properties of unidirectional piezofiber composites, and also possibly over those of single-phase piezoelectric materials. The proposed LPC has a two-scale structure: it consists of two alternating layers, where each layer is a piezoelectric fiber composite with continuous fibers of an elliptical cross section forming a herringbone mesostructure with the fibers in the neighboring layers. The optimal design of the herringbone mesostructure of these composites offers the potential to considerably improve the effective properties of these composites for energy harvesting purposes. Composites with a herringbone mesostructure have been investigated before in different contexts. For example, Milton [14] introduced a two-phase elastic composite with hexagonal symmetry (resembling a herringbone mesostructure) that can possess negative overall Poisson's ratios. The herringbone mesostructure was also recently investigated in the context of elastomeric magnetoactive actuators [15], and it was shown that the composites with this mesostructure can achieve strain as high as 100%.

This paper is organized as follows. Section II addresses the local constitutive relations for the piezoelectric fibers and the inactive matrix, and it describes the laminated structure considered in this work. In Sec. III, we lay out a two-step homogenization procedure to obtain the effective properties of the laminated composites. In Sec. IV, we provide examples illustrating the consistent improvement of the effective piezoelectric properties of these composites, including effective piezoelectric charge and voltage coefficients, as well as effective electromechanical coupling factors for two in-plane operation modes. The representative examples are given for a wide range of microstructural parameters, such as shape, volume fraction, and orientation of the fibers. For the special case of these composites when the fibers approach a layer shape, we will fine-tune the orientation of the fibers to obtain optimal values of the effective electromechanical factors of these composites. Finally, some conclusions are drawn in Sec. V.

II. LOCAL PROPERTIES AND STRUCTURE

Consider a double-layered laminated composite that consists of two alternating layers of piezoelectric materials. Each layer is a random piezoelectric composite consisting of an isotropic linear-elastic matrix and aligned, continuous cylindrical piezoelectric fibers of an elliptical cross section with an aspect ratio $\alpha > 0$. We assume that, in each layer, the aligned fibers are distributed with elliptical symmetry in the plane transverse to the fiber direction; however, the initial in-plane orientation of fibers in two adjacent layers are different. Figure 1 shows a schematic representation of the transverse cross section of the microstructure. For definiteness, we use the global Cartesian basis $\{\mathbf{e}_i\}$, $i = 1, 2, 3$, such that the lamination direction (denoted by $\mathbf{N}$) and the longest axis of the fibers are aligned with the $\mathbf{e}_2$ and $\mathbf{e}_3$ directions, respectively. As shown in Fig. 1, the fibers in the adjacent layers represent a herringbone mesostructure such that they are oriented at angles θ and $-\theta$ relative to the axis $\mathbf{e}_2$. However, the local constitutive properties, the shape, and the volume fractions of the fibers are kept the same in both layers to maintain orthotropic symmetry in the effective properties of the laminate. In addition, we assume that multiple length scales in the laminate are well separated. Indeed, the typical size of the fibers is much smaller than the typical thickness of the layers which, in turn, is assumed to be much smaller than the size of the laminate. We refer to these three characteristic sizes as microscale, mesoscale, and macroscale, respectively.

The piezoelectric fibers exhibit linear, anisotropic coupling between an electric field and elastic deformation, characterized by the negative gradient of the electric potential, $E = -\nabla\phi$, and the infinitesimal strain tensor $\boldsymbol{\varepsilon}$, respectively. The constitutive relations for the fibers can be written in tensor notation as

$$\begin{aligned} \sigma_{ij} &= C_{ijkl}\varepsilon_{kl} - e_{kij}E_k, \\ D_i &= e_{ikl}\varepsilon_{kl} + K_{ik}E_k, \end{aligned} \tag{1}$$

where $\boldsymbol{\sigma}$ and $\mathbf{D}$ are the Cauchy stress tensor and the electric-displacement vector, respectively, $\mathbf{C}$ is the fourth-order tensor of elastic moduli at a fixed electric field, $\mathbf{K}$ is the

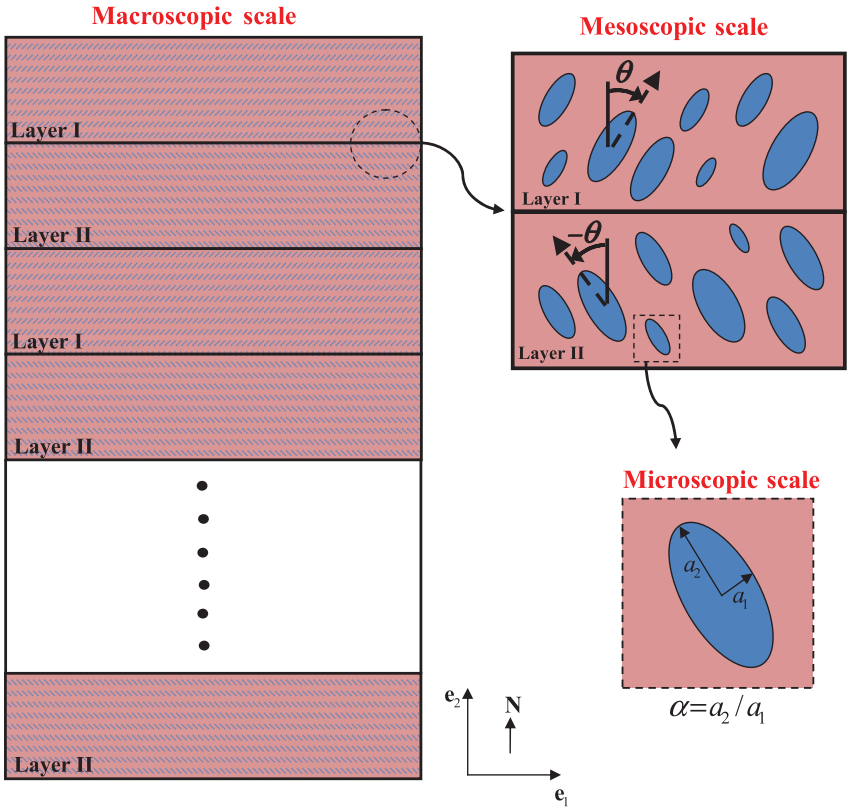

FIG. 1. Schematic representation of the microstructure and mesostructure in the "laminated piezoelectric composite." The LPC consists of two alternating layers (mesoscale) where each is made of a distribution of a polymeric matrix and long, unidirectional piezoelectric fibers (microscale).

second-order permittivity tensor at a fixed strain, and $\mathbf{e}$ is the third-order tensor of piezoelectric constants characterizing coupling between the electric field and elastic deformation. For future reference, we note that two alternative forms of the piezoelectric constitutive equations (1) involving the piezoelectric charge and voltage tensors (i.e., $\mathbf{d}$ and $\mathbf{g}$) are discussed in Appendix A with relationships between the coupling tensors. However, we choose the form (1) for performing standard homogenization techniques in the next section, and other important electromechanical properties can be calculated using the relationships provided in Appendix A.

For convenience in our homogenization analysis in the next section, we adopt a shorthand notation introduced by Barnett and Lothe [16] to represent the constitutive relations in a unified single equation. To do so, the field variables of the material take the following shorthand forms:

$$\Sigma_{iJ} = \begin{cases} \sigma_{ij} & J = 1,2,3 \\ D_i & J = 4 \end{cases}, \qquad Z_{Kl} = \begin{cases} \varepsilon_{kl} & K = 1,2,3 \\ -E_l & K = 4 \end{cases}. \tag{2}$$

Herein, the lowercase subscripts range from 1 to 3, and the uppercase ones from 1 to 4, with the subscript 4 referring to the piezoelectric quantities. Accordingly, the electromechanical moduli are expressed in a compact matrix as

$$L_{iJKl} = \begin{cases} C_{ijkl} & J,K = 1,2,3 \\ e_{lij} & J = 1,2,3 \quad K = 4 \\ e_{ikl} & J = 4 \quad K = 1,2,3 \\ -K_{il} & J,K = 4 \end{cases}. \tag{3}$$

With this set of notations, the linear constitutive relations are shortened to

$$\Sigma_{iJ} = L_{iJKl} Z_{Kl}. \tag{4}$$

As mentioned before, the matrix phase is assumed to be an isotropic linear-elastic material. Therefore, its constitutive behavior can be described by relations (2) and (3), with specializations of $e_{ijk} = 0$ and $K_{ij} = K_0 \mathbf{I}$, where $K_0 = 8.85 \times 10^{-12}\,(\mathrm{C}^2/\mathrm{Nm}^2)$ is the permittivity of free space.

For definitiveness, we use the superscripts (1) and (2) to denote variables associated with the matrix and piezoelectric fibers within a layer, respectively. Also, we use the superscripts (I) and (II) to distinguish between the (mesoscale) variables associated with layers I and II, respectively (see Fig. 1.)

III. EFFECTIVE RESPONSE: TWO-STEP HOMOGENIZATION

As mentioned earlier, we assume that the characteristic size of the piezoelectric fibers, the thickness of individual

layers, and the size of the laminated specimen are well separated. In addition, we assume that the thickness of the layers is much smaller than the scale of variation of the loading conditions applied to the laminate. Following these assumptions, we will be able to obtain the effective piezoelectric properties of the laminate by performing two homogenizations: first, over a single layer (consisting of a polymeric matrix and piezoceramic fibers) and, second, over the entire laminate (consisting of already-homogenized piezoelectric layers). The first homogenization will provide us with the effective properties of each layer which will be used as mesoscale properties in the second homogenization to obtain the effective properties of the laminate.

Dunn and Taya [11] extended the application of several homogenization techniques, including Mori-Tanaka, self-consistent, and differential micromechanical methods to estimate effective electroelastic properties of piezoelectric composites. These approximate methods (which were mainly explored in the context of linear-elastic composites) are based on the Eshelby solution [17] for a single inclusion of ellipsoidal shape embedded in an infinite matrix subjected to uniform fields at infinity. Following the work of Deeg [18], Dunn and Taya [11,19] extended these methods by treating elastic and electric variables in a similar way and recasting the original micromechanical formulation in a unified matrix representation. Among other applications, they studied (long) piezoelectric fiber composites and concluded that the Mori-Tanaka scheme achieves better agreement with experiments up to a relatively high concentration of fibers.

Based on these considerations, in this work, we will use the Mori-Tanaka method [20] to obtain the effective piezoelectric properties of fiber-reinforced layers, i.e., mesoscale properties of the laminate. Moreover, as we discuss further in this section, the rank-1 laminate microstructure is a limiting case of an ellipsoidal microstructure where two aspect ratios of ellipsoidal inclusions tend to infinity and the inclusions become layers. Therefore, having obtained the effective properties of both layers, we similarly use the Mori-Tanaka homogenization formulation for laminate microstructures to obtain macroscopic properties of the LPC. In this connection, we note that *exact* analytical estimates for the effective electroelastic behavior of piezoelectric laminated composites can be derived based on the exact uniform-field solution within the layers. However, it is known that the Mori-Tanaka formulation for ellipsoidal microstructures reduces to these exact estimates in the limiting case of (rank-1) laminate microstructures [21]. In the following subsections, we present the related formulations for each homogenization.

A. First homogenization: From microscale to mesoscale

Assuming perfect bonding between the matrix and the fibers, the electroelastic fields of the composite at the mesoscale (i.e., at the length scale of individual layers) can be expressed as [11]

$$\bar{\boldsymbol{\Sigma}}^{\text{meso}} = (1-c)\bar{\boldsymbol{\Sigma}}^{(1)} + c\bar{\boldsymbol{\Sigma}}^{(2)},$$
$$\bar{\mathbf{Z}}^{\text{meso}} = (1-c)\bar{\mathbf{Z}}^{(1)} + c\bar{\mathbf{Z}}^{(2)}, \tag{5}$$

where c is the volume fraction of the piezofibers, the subscript meso denotes the effective variables at the mesoscale, and the overbar denotes the volume average over the respective scale. The effective constitutive equation for the piezoelectric layers can be expressed in terms of the volume-averaged fields:

$$\bar{\boldsymbol{\Sigma}}^{\text{meso}} = \tilde{\mathbf{L}}^{\text{meso}}\bar{\mathbf{Z}}^{\text{meso}}, \tag{6}$$

where $\tilde{\mathbf{L}}^{\text{meso}}$ is the effective electromechanical moduli matrix of an individual layer. Following the Mori-Tanaka approach [11,20], the effective moduli $\tilde{\mathbf{L}}^{\text{meso}}$ is obtained as

$$\tilde{\mathbf{L}}^{\text{meso}} = \mathbf{L}^{(1)} + c[(\mathbf{L}^{(2)} - \mathbf{L}^{(1)})^{-1} + (1-c)\mathbf{S}^{F}(\mathbf{L}^{(1)})^{-1}]. \tag{7}$$

In the above relation, the $\mathbf{S}^{F}$ is the electroelastic Eshelby matrix (also known as the constraint tensor [11]) which is a function of the shape of the elliptical fibers and the elastic properties of the inactive (polymeric) matrix. Discussions on explicit expressions for $\mathbf{S}^{F}$ are provided in Appendix B. Also, it is important to note that the above Mori-Tanaka estimate does not incorporate information on the distribution of piezolectric fibers in the microscale. Variational bounds that can account for both the particle shape and the two-point distribution function are available in the purely elastic and dielectric cases [22,23], and they are yet to be developed for the general piezoelectric composites.

B. Second homogenization: From mesoscale to macroscale

As discussed earlier, we assume that the length scales of the piezoelectric fibers (the microstructure) and the layers (the mesostructure) are well separated. As a result, the laminated composite can be modeled as a doubly layered composite where the behavior of each layer is described by the constitutive relation (6). The (homogenized) constitutive relations for layers I and II in the fixed global-coordinate basis $\{\mathbf{e}_i\}$ $(i = 1, 2, 3)$ can be written as

$$\bar{\Sigma}_{iJ}^{(\text{I})} = \tilde{L}_{iJKl}^{(\text{I})}\bar{Z}_{Kl}^{(\text{I})},$$
$$\bar{\Sigma}_{iJ}^{(\text{II})} = \tilde{L}_{iJKl}^{(\text{II})}\bar{Z}_{Kl}^{(\text{II})}, \tag{8}$$

where the meso superscript is dropped from all variables for simplicity. In the above equation, the compact matrices $\tilde{L}_{iJKl}^{(\text{I})}$ and $\tilde{L}_{iJKl}^{(\text{II})}$ (with components relative to the basis $\{\mathbf{e}_i\}$) are obtained by appropriate transformation rules,

$$\tilde{L}^{(\mathrm{I,II})}_{iJKl} = \begin{cases} Q^{(\mathrm{I,II})}_{ir} Q^{(\mathrm{I,II})}_{js} Q^{(\mathrm{I,II})}_{kp} Q^{(\mathrm{I,II})}_{lq} \tilde{C}^{\mathrm{meso}}_{rspq} & J,K = 1,2,3 \\ Q^{(\mathrm{I,II})}_{lr} Q^{(\mathrm{I,II})}_{is} Q^{(\mathrm{I,II})}_{jp} \tilde{e}^{\mathrm{meso}}_{rsp} & J = 1,2,3 \quad K = 4 \\ Q^{(\mathrm{I,II})}_{ir} Q^{(\mathrm{I,II})}_{ks} Q^{(\mathrm{I,II})}_{lp} \tilde{e}^{\mathrm{meso}}_{rsp} & J = 4 \quad K = 1,2,3 \\ -Q^{(\mathrm{I,II})}_{ir} Q^{(\mathrm{I,II})}_{ls} \tilde{K}^{\mathrm{meso}}_{rs} & J,K = 4 \end{cases}, \tag{9}$$

where $\tilde{C}^{\mathrm{meso}}_{rspq}$, $\tilde{e}^{\mathrm{meso}}_{ijk}$, and $\tilde{K}^{\mathrm{meso}}_{ij}$ are components of the moduli $\tilde{\mathbf{L}}^{\mathrm{meso}}$ [according to definition (3)] in the principal fiber axes, and the orthogonal matrices of $Q^{(\mathrm{I})}_{ij}$ and $Q^{(\mathrm{II})}_{ij}$ are given by

$$\begin{aligned} Q^{(\mathrm{I})}_{ij} &= \cos(\theta)(\mathbf{e}_1 \otimes \mathbf{e}_1 + \mathbf{e}_2 \otimes \mathbf{e}_2) \\ &\quad + \sin(\theta)(\mathbf{e}_1 \otimes \mathbf{e}_2 - \mathbf{e}_2 \otimes \mathbf{e}_1), \\ Q^{(\mathrm{II})}_{ij} &= \cos(\theta)(\mathbf{e}_1 \otimes \mathbf{e}_1 + \mathbf{e}_2 \otimes \mathbf{e}_2) \\ &\quad + \sin(\theta)(\mathbf{e}_2 \otimes \mathbf{e}_1 - \mathbf{e}_1 \otimes \mathbf{e}_2). \end{aligned} \tag{10}$$

The volume-averaged (macroscopic) piezoelectric fields $\bar{\mathbf{\Sigma}}$ and $\bar{\mathbf{Z}}$ are written in terms of the averages of the corresponding mesoscale fields:

$$\begin{aligned} \bar{\mathbf{\Sigma}} &= 0.5(\bar{\mathbf{\Sigma}}^{(\mathrm{I})} + \bar{\mathbf{\Sigma}}^{(\mathrm{II})}), \\ \bar{\mathbf{Z}} &= 0.5(\bar{\mathbf{Z}}^{(\mathrm{I})} + \bar{\mathbf{Z}}^{(\mathrm{II})}). \end{aligned} \tag{11}$$

Considering an affine boundary condition, the effective constitutive behavior of the LPC can be defined as

$$\bar{\mathbf{\Sigma}} = \tilde{\mathbf{L}}\,\bar{\mathbf{Z}}, \tag{12}$$

where $\tilde{\mathbf{L}}$ is the effective electromechanical moduli. The effective behavior of composites with perfectly layered microstructures can be computed exactly [24] thanks to the essential feature of these composites: that the local fields (such as stress, strain, electric, etc.) are constant in each layer. Making use of this feature, the associated homogenization problem reduces to solving appropriate (displacement, stress, and electric) boundary and jump conditions across the layer interfaces which constitute a set of linear algebraic equations. For a two-phase laminate (which is our case in this work), a simpler approach to find the effective electromechanical behavior of the laminate is to make use of the Mori-Tanaka estimate with the appropriate Eshelby matrix. More specifically, as is discussed in Appendix B, the Eshelby matrix for 2D laminate structure (denoted by $\mathbf{S}^L$) can be simply obtained from the Eshelby matrix of elliptical geometry by taking the limit as the aspect ratio goes to zero. Therefore, following this approach, the Mori-Tanaka estimate for the two-phase laminate with moduli matrices $\mathbf{L}^{(\mathrm{I})}$ and $\mathbf{L}^{(\mathrm{II})}$ and the equal volume fraction for the phases read as

$$\tilde{\mathbf{L}} = \mathbf{L}^{(\mathrm{I})} + [2(\mathbf{L}^{(\mathrm{II})} - \mathbf{L}^{(\mathrm{I})})^{-1} + \mathbf{S}^L(\mathbf{L}^{(\mathrm{I})})^{-1}]. \tag{13}$$

It is important to note that the above Mori-Tanaka estimate is consistent with the exact solutions for the laminated structure [21]. In summary, for given microstructural parameters c and α and the local properties $\mathbf{L}^{(1)}$ and $\mathbf{L}^{(2)}$, the effective moduli matrix $\tilde{\mathbf{L}}$ of the LPC is obtained in two steps: (i) determining the moduli matrices $\mathbf{L}^{(\mathrm{I})}$ and $\mathbf{L}^{(\mathrm{II})}$ of two alternating layers from relations (7) and (9), and (ii) substituting the former matrices in relation (13). Once the moduli matrix $\tilde{\mathbf{L}}$ is calculated, the effective electromechanical properties are obtained from relations (2).

IV. RESULTS AND DISCUSSIONS

In this subsection, we provide some representative results illustrating the improvement of the effective electrostatic properties of the proposed laminated composite for energy harvesting purposes. Specifically, we explore the effects of the microstructural parameters including the 2D orientation angle of the piezoelectric fibers, the aspect ratio, and the volume fraction of the fibers. We will demonstrate the significant effect of these parameters on improving the effective properties of the laminated composite. For all examples considered here, the piezoelectric phase is taken to be transversely isotropic, with the poling direction pointing along the local direction $\mathbf{e}'_2$ [see Fig. 2(a)]. The material properties for the polymeric matrix (epoxy) and piezoelectric fibers (PZT-7A) used in the calculations are listed in Table I relative to the principal axes of the fibers.

As mentioned earlier, the coupled charge and voltage piezoelectric coefficients (the components $\tilde{d}_{ijk}$ and $\tilde{g}_{ijk}$, respectively) are of critical importance for energy harvesting applications. As is discussed in Appendix A, these tensors can be calculated in terms of the homogenized tensors $\tilde{\mathbf{e}}$, $\tilde{\mathbf{C}}$, and $\tilde{\boldsymbol{\beta}}$ using the same relationships as for the case of homogeneous piezoelectric materials. Here, we assume a static frequency condition and consider operation modes of 21 and 22 that correspond to collecting electrical energy in the $\mathbf{e}_2$ direction when the mechanical forces are applied in the $\mathbf{e}_1$ and $\mathbf{e}_2$ directions, respectively. Figure 2 shows schematic representations of these operation modes. The relevant components of the tensors $\tilde{\mathbf{d}}$ and $\tilde{\mathbf{g}}$ for operation modes of 21 and 22 are the pairs of $(\tilde{d}_{21}, \tilde{g}_{21})$ and $(\tilde{d}_{22}, \tilde{g}_{22})$, respectively. Here, we have used the reduced

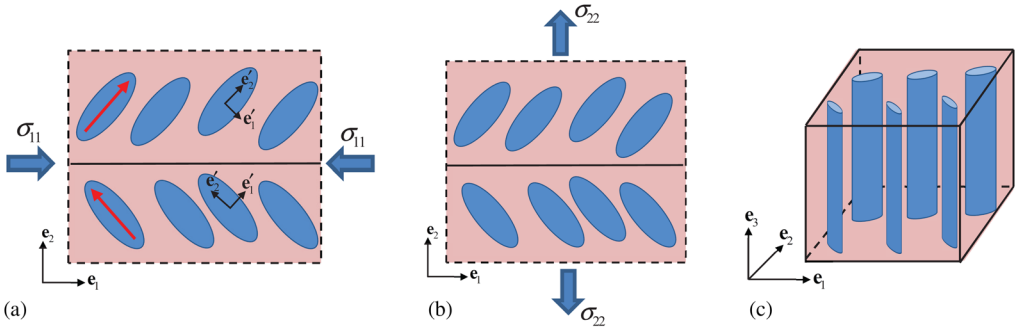

FIG. 2. Schematic representation of energy harvesting operation modes. (a) Mode 21. (b) Mode 22. (c) Three-dimensional geometry.

notation where the first and second subscripts denote the directions along which the electrical energy is collected and the mechanical force is applied, respectively. Moreover, we note that all of the results for the effective properties $\tilde{d}_{ijk}$ and $\tilde{g}_{ijk}$ are normalized by the corresponding properties of the piezoelectric fibers. This normalization provides a clear perspective on the level of improvement in the effective properties of the LPC. Before proceeding with the results, it is also worth remarking on the connection between Mori-Tanaka estimates shown in this work and available bounds for piezoelectric composites. Based on the results of Yu Li and Dunn [25], the Mori-Tanaka estimates for the two-phase LPCs having fibers as the stiffer phase (which is the case here, as detailed in Table I) correspond to the Hashin-Shtrikman lower bound for such composites. However, we add that the available Voigt-Reuss and Hashin-Shtrikman bounds for piezoelectric composites [25,26] are mainly pertinent to diagonal tensors in the effective electromechanical moduli $\tilde{\mathbf{L}}$, and they serve only as estimates for the off-diagonal tensors such as $\tilde{\mathbf{d}}$ and $\tilde{\mathbf{g}}$ [25]. In any event, we remind that the results for the limiting case of laminate composites ($\alpha \to 0,\ \infty$) are exact and would correspond to both the Hashin-Shtrikman lower and upper bounds.

First, we investigate the effect of the microstructure on the behavior of the aforementioned individual components of $\tilde{\mathbf{d}}$ and $\tilde{\mathbf{g}}$. Figure 3 shows plots for the components of $\tilde{\mathbf{d}}$ and $\tilde{\mathbf{g}}$ related to the operation mode of 21 as a function of θ. The results are given for the fixed volume fraction $c = 0.6$, and various values of the fiber aspect ratio (α) ranging from 0 to ∞. We note that the special cases of $\alpha = 1$ and $\alpha \to 0$, ∞ correspond to circular fibers and a laminated microstructure, respectively. An important overall observation from this figure is that, as the aspect ratio of the fiber deviates from a circular shape, the effective properties show a progressively stronger variation with orientation of the fibers, and they reach a maximum at certain values of the orientation angle. For the case of $\alpha \leq 1$, we observe from Figs. 3(a) and 3(b) that the normalized components $\tilde{d}_{21}/d_{21}^{(2)}$ and $\tilde{g}_{21}/g_{21}^{(2)}$ both reach maximum values of greater than one for the laminated case of $\alpha \to 0$. In this case, $\tilde{d}_{21}/d_{21}^{(2)}$ exhibits a considerable increase relative to the case of the circular fibers ($\alpha = 1$), while $\tilde{g}_{21}/g_{21}^{(2)}$ increases only by multiple folds. For the case of $\alpha \geq 1$, we similarly observe from Figs. 3(c) and 3(d) that, as the piezoelectric fibers approach a platelike shape $\alpha \to \infty$, a herringbone mesostructure at certain angles can notably increase the magnitude of the overall piezoelectric constants of the composite compared to the case of the circular fibers ($\alpha = 1$). In this case, $\tilde{g}_{21}/g_{21}^{(2)}$ shows a stronger variation with the shape of the fibers in contrast to the case of $\alpha \leq 1$. Moreover, it is interesting to note from all of the figures that the effective constants for the case of $\alpha = 1$ also vary by the angle θ, which, in this case, characterizes the dipole direction of circular fibers in layers I and II [see Fig. 2(a)]. All constants become zero at $\theta = 90°$ since the dipoles in two layers take opposing directions [see Fig. 2(a)]. Lastly, we remark that the question of why a herringbone mesostructure can increase overall piezoelectric properties remains to be fully explored; however, our preliminary calculations suggest that such a mesostructure increases the stress concentration in the piezoelectric fibers, which leads to a more sensitive piezoelectric composite. This mechanism is similar to changing the shape of the fibers from circular to elliptical, which leads to higher stress concentrations and, ultimately, higher charge and voltage piezoelectric properties, as seen in Figs. 3(c) and 3(d) at $\theta = 0°$.

TABLE I. Electromechanical properties of candidate materials for the piezoelectric fibers and the polymeric matrix in the LPC. The dimensions are C_{ijkl}(GPa), e_{ijk}(C/m^2), and $K_0 = 8.85 \times 10^{-12}$ (C^2/N m^2). The properties are given relative to the local basis $\{\mathbf{e}_i'\}$ shown in Fig. 2(a). Note that the fibers are elastically transversely isotropic around the local axis $\mathbf{e}_2'$.

Properties	C_{1111}	C_{1122}	C_{1133}	C_{2222}	C_{1212}	e_{211}	e_{222}	e_{112}	K_{11}/K_0	K_{22}/K_0
PZT-7A	148	74.2	76.2	131	25.4	−2.1	9.5	9.2	460	235
Epoxy	8	4.4	4.4	8	1.8	0	0	0	4.2	4.2

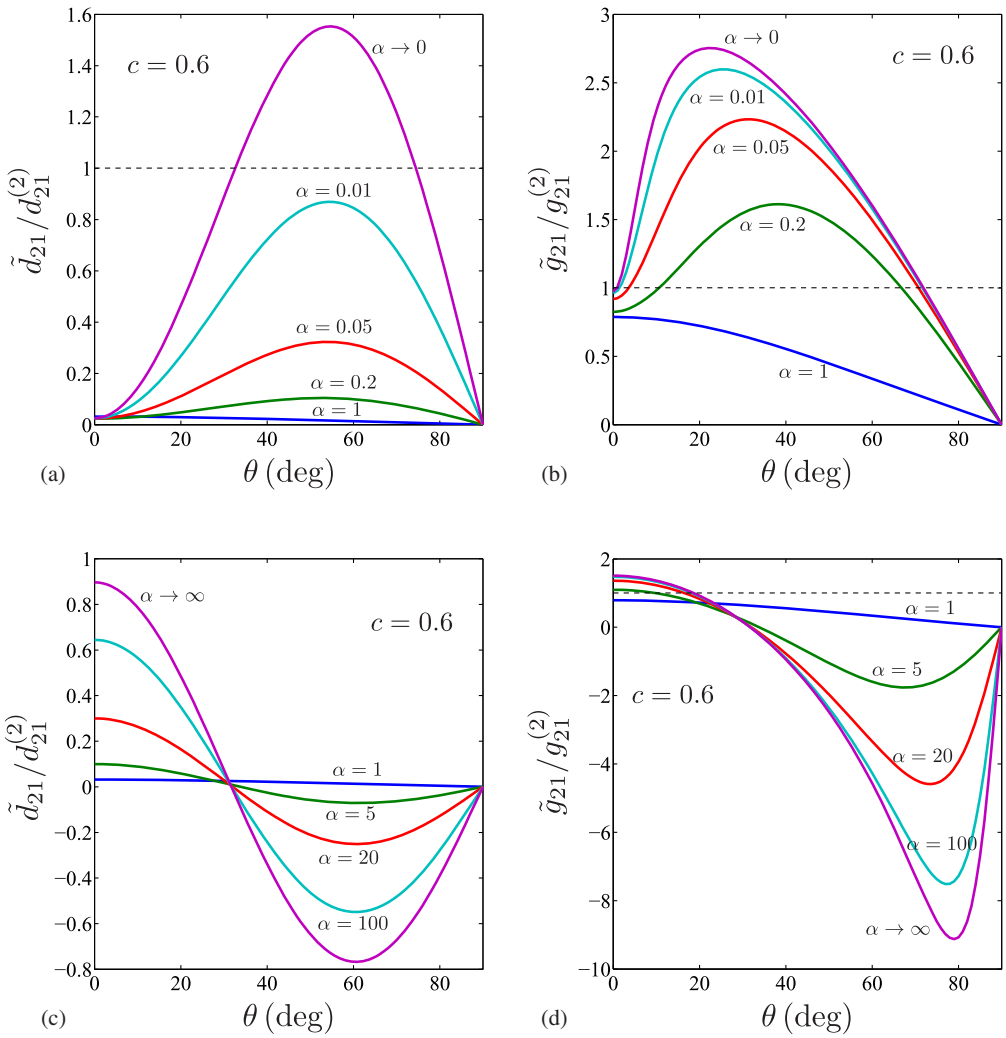

FIG. 3. Estimates for the effective piezoelectric properties of a LPC with $c = 0.6$ and various values of the aspect ratio α for an operation mode of 21. (a),(b) Effective charge and voltage constants for $\alpha \leq 1$. (c),(d) Effective charge and voltage constants for $\alpha \geq 1$.

The results in Fig. 3 suggest that the maximum effect of the herringbone arrangement takes place for the special case of $\alpha \to 0$ where the fibers become layers. For this reason, henceforth, all results are presented for this special case. Figure 4 shows a schematic representation of the mesostructure of the LPC in this limiting case. Here, it is worth briefly remarking on the manufacturing of the proposed multilayered composite in Fig. 4. Such composites can be manufactured in a sequential manner [15]. Indeed, a mesoscale laminate consisting of alternating monolayers of piezoelectric and epoxy phases (microscale) could be fabricated by stacking the layers on top of each other (to make it several times thicker than monolayers). The stacking should follow the appropriate angle calculated from theoretical design. Finally, these thicker mesolayers should be stacked by alternating the orientation and glued together by conductive adhesive to generate materials with the desired herringbone structure. However, it is important to contrast the manufacture of such multiscale composites to that of traditional piezofiber composites with aligned circular or elliptical fibers. In fact, such a sequential stacking procedure seems to be easier than producing unidirectional piezofiber composites with all fiber having the same in-plane or out-of-plane poling direction.

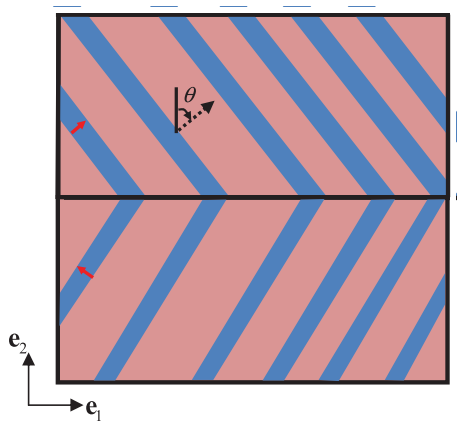

FIG. 4. Schematic representation of the laminated microstructure corresponding to the special case of $\alpha \to 0$.

Next, in Fig. 5, we investigate the effect of the volume fraction of piezoelectric fibers on the normalized values of

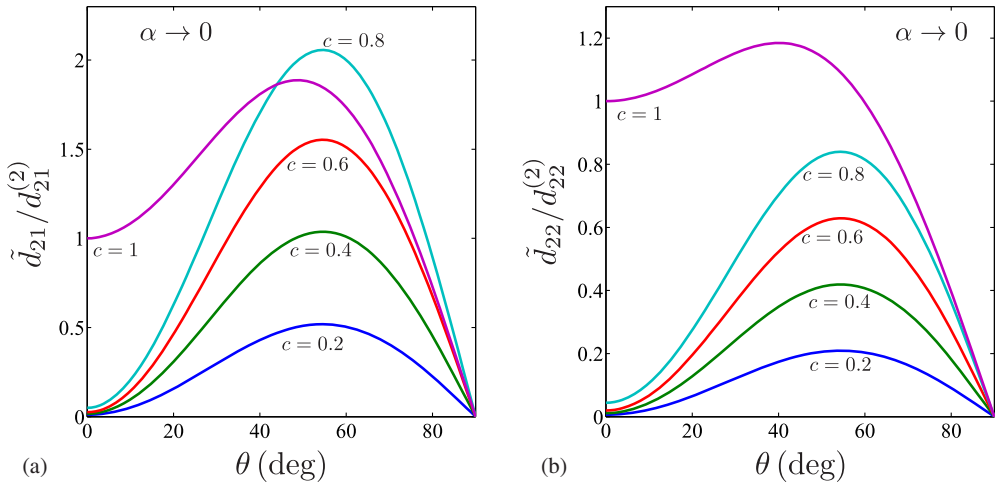

FIG. 5. Estimates for the effective charge piezoelectric properties of a LPC with $\alpha \to 0$ for various values of c. (a) Mode 21. (b) Mode 22.

the coefficients $\tilde{d}_{21}$ and $\tilde{d}_{22}$. The results are given for five values of c—0.2, 0.4, 0.6, 0.8, and 1—as functions of θ. A general observation from this figure is that the herringbone hierarchy can produce a stronger effect on the overall charge piezoelectric coefficients as the volume fraction of the fiber increases. Specifically, we observe from Fig. 5(a) that the coefficient $\tilde{d}_{21}$ can reach values as large as 2 times the value of the corresponding coefficient of the single-phase piezoelectric material by increasing the volume fraction c to 0.8. Here, it is important to clarify that, although such hierarchical piezoelectric composites provide a modest improvement over single-phase piezoelectric materials, their greatest strength is to serve as an improved alternative to unidirectional piezofiber-polymeric-matrix composites for applications in which the use of polymer-based composites is critical to ensure environmental compatibility and flexibility. With this perspective in mind, we infer by comparing the results in Fig. 5(a) to the result for $\alpha = 1$ in Fig. 3(a) that, even for smaller values of the fiber volume fraction, introducing a herringbone mesostructure in piezofiber composites can greatly improve the overall piezoelectric coefficients over those for the case of circular-fiber composites. Finally, it is interesting to observe from both Fig. 5(a) and Fig. 5(b) that even stacking single-phase piezoelectric layers with their dipole directions set in a herringbone arrangement (i.e., the case of $c = 1$) can lead to higher overall piezoelectric coefficients than those of constituent piezoelectric materials.

Next, we focus on finding the optimal value of the orientation angle θ for the maximal performance of the LPCs for energy harvesting. For this purpose, we study the electromechanical coupling factor (denoted by k), which is an indicator of the effectiveness of a piezoelectric material to convert electrical energy into mechanical energy [27–29]. At low input frequencies, the coupling factors associated with the operation modes 21 and 22 are defined as [27]

$$\tilde{k}_{21} = \sqrt{\frac{\tilde{d}_{211}^2}{\tilde{M}_{1111}\,\tilde{K}_{22}^S}} = \sqrt{\frac{\tilde{d}_{211}\tilde{g}_{211}}{\tilde{M}_{1111}}},$$
$$\tilde{k}_{22} = \sqrt{\frac{\tilde{d}_{222}^2}{\tilde{M}_{2222}\,\tilde{K}_{22}^S}} = \sqrt{\frac{\tilde{d}_{222}\tilde{g}_{322}}{\tilde{M}_{2222}}}, \qquad (14)$$

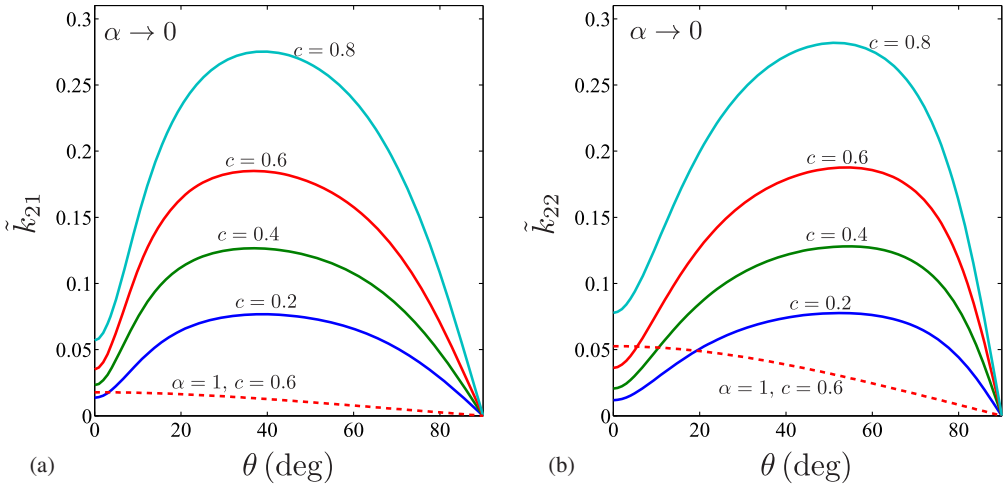

FIG. 6. Estimates for the effective electromechanical coupling factors of a LPC with $\alpha \to 0$ for various values of c. (a) Mode 21. (b) Mode 22. Corresponding estimates for the case of circular fibers with $c = 0.6$ are included for comparison purposes.

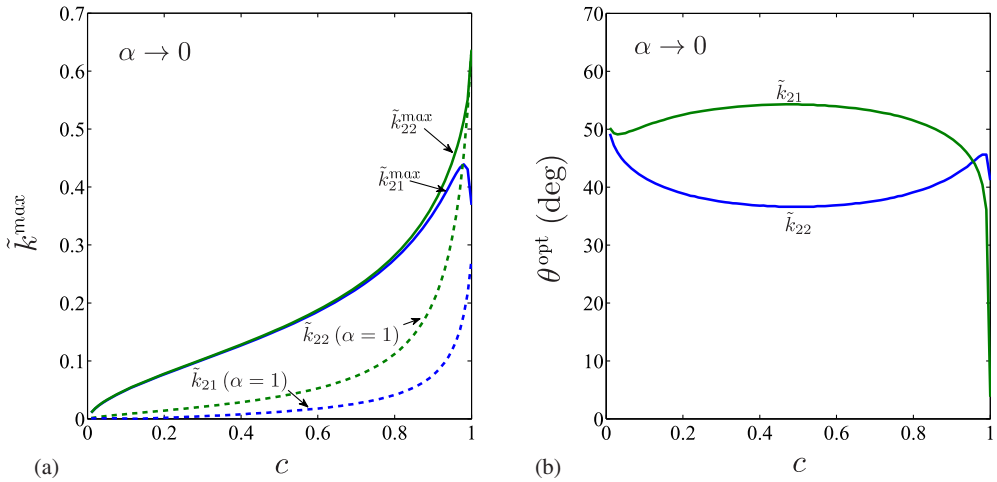

FIG. 7. Optimization of the effective electromechanical coupling factors of a LPC with $\alpha \to 0$ as a function of c. (a) Optimal values of the electromechanical coupling factors. (b) The values of the angle θ at which the factor is optimized.

respectively, where $\tilde{M}_{ijkl}$ and $\tilde{K}^S_{ij}$ are the effective compliance and permittivity tensors of the LPC, at constant electric field and constant stress, respectively. In the above relations, use has been made of relation (A3). Note that $\tilde{k}$'s factors assume a value between zero and one.

Figure 6 shows plots for the factors $\tilde{k}_{21}$ and $\tilde{k}_{22}$ as a function of θ. The results are given for LPCs with $\alpha \to 0$ and several values of the volume fraction. It can be seen from these figures that the effective coupling factors of the LPCs with herringbone mesostructure can achieve noticeably higher values than those of the circular piezoelectric fiber composites (shown in dashed lines for $c = 0.6$) at certain values of the orientation angle θ. Once again, this observation suggests that laminated composites with herringbone mesostructure offer higher performance over traditional piezofiber composites, even when a smaller fraction of piezoelectric ceramic layers is used. Specifically, as can be seen from Figs. 6(a) and 6(b), the factors $\tilde{k}_{21}$ and $\tilde{k}_{22}$ attain there maximum values at the layer orientation $\theta \approx 40°$ and $\theta \approx 60°$, respectively.

Finally, in Fig. 7, we optimize the effective factors $\tilde{k}_{21}$ and $\tilde{k}_{22}$ with respect to θ as a function of c. Specifically, Fig. 7(a) shows the maximum values of coupling factors, while Fig. 7(b) shows the corresponding optimal values of the orientation θ at which maximum $\tilde{k}$'s are achieved. Again, the results correspond to the case of $\alpha \to 0$. Also, in Fig. 7(a), for comparison purposes, we have included estimates for the case of circular fibers ($\alpha = 1$) at $\theta = 0°$ corresponding to the case in which all fibers have the same dipole direction towards $\mathbf{e}_2$ [see Fig. 2(a)]. We observe from Fig. 7(a) that, for a piezoelectric composite with a fixed volume fraction c, a notably higher value of the coupling factors can be achieved by using a herringbone mesostructure at an optimized orientation θ^{opt}, calculated in Fig. 7(b). However, the maximum values of the coupling factors (over all volume fractions) are obtained close to $c = 1$. This observation suggests that, for applications in which the use of polymer-matrix piezoelectric composites is not important, other nonfibrous composites such as piezoelectric lattices [30,31] that offer significant improvements over single-phase composites could be better alternatives. Finally, it is interesting to observe from Fig. 7(a) that the maximum value of $\tilde{k}_{21}$ occurs slightly before $c = 1$, with $\theta^{opt} \approx 45°$, while the maximum value of $\tilde{k}_{22}$ occurs exactly at $c = 1$, with $\theta^{opt} = 0°$. It is further interesting to note that, at $c = 1$, a composite with a herringbone arrangement of single-phase piezoelectric phases with $\theta \approx 40°$ again leads to a higher $\tilde{k}_{21}$ than a single-phase piezoelectric with a fixed dipole direction (shown with a dashed line).

V. CONCLUDING REMARKS

We present a class of LPCs consisting of a polymeric matrix and elliptical piezoelectric fibers with herringbone mesostructures that offer significantly greater energy harvesting performance than that of unidirectional piezofiber composites for operation modes 21 and 22. We demonstrate that, for the limiting case in which all fibers tend to a platelike shape (and the LPC becomes a rank-2 laminate), the composite can possess piezoelectric properties, including both charge and voltage coefficients, even higher than those of the constituent fibers for operation mode 21. Although increases in the latter are modest, the greatest strength of the proposed composites remains to be the superiority over unidirectional piezofiber composites for applications in which the use of a polymer-matrix composite is critical for environmental compatibility, durability, and flexibility. Also, we show that this class of composites can have consistently higher electromechanical coupling factors than those of unidirectional piezofiber composites. In addition, the proposed rank-2 laminated composite offers a relatively easy manufacturing process. The optimal design of the microstructural variables, such as the fiber shape, volume fraction, and orientation in the LPC composites, offers an opportunity

for enhancement of the overall piezoelectric performance. Specifically, optimal values of the effective electromechanical properties always take place in the limiting case of piezoelectric layers, where the LPC becomes a rank-2 laminate. Lastly, we find that stacking single-phase piezoelectric ceramics on top of each other, such that their dipole direction takes a herringbone arrangement, can lead to a higher piezoelectric sensitivity than that of a single-phase ceramic with a uniform dipole direction. In future work, we expect to investigate the optimal microstructural geometry for multiferroic composites with active particles [12,32] to achieve enhanced coupled properties for applications in sensors. Overall, such studies open up frontiers to investigate the effect of hierarchical geometry on improving the coupled behavior of smart materials for power-harvesting, sensing, and actuating applications.

APPENDIX A: ALTERNATIVE FORMS OF THE CONSTITUTIVE RELATION (1)

In this appendix, we express two alternative forms for the constitutive equations (1) and for useful relations between the electromechanical properties. These two forms can be expressed as

$$\begin{aligned} \varepsilon_{ij} &= M_{ijkl}\sigma_{kl} + d_{kij}E_k, \\ D_i &= d_{ikl}\sigma_{kl} + K^S_{ik}E_k \end{aligned} \tag{A1}$$

and

$$\begin{aligned} \varepsilon_{ij} &= M^D_{ijkl}\sigma_{kl} + g_{kij}D_k, \\ E_i &= -g_{ikl}\sigma_{kl} + \beta_{ik}D_k, \end{aligned} \tag{A2}$$

where d_{ikl} and g_{kij} are alternative forms of the piezoelectric tensor, K^S_{ik} and β_{ik} are the permittivity and impermittivity tensors at constant stress, respectively, and M_{ijkl} and M^D_{ijkl} are the elastic compliance tensors at a constant electric field and a constant electric displacement, respectively.

The relations between the piezoelectric coefficients appearing in the three sets of constitutive equations [relations (1), (A1), and (A2)] may be written as

$$\mathbf{d} = (\mathbf{C})^{-1}\mathbf{e}, \qquad \mathbf{g} = \mathbf{d}\boldsymbol{\beta}, \tag{A3}$$

where $\boldsymbol{\beta} = (\mathbf{K}^S)^{-1} = [\mathbf{K} + \mathbf{e}^t(\mathbf{C})^{-1}\mathbf{e}]^{-1}$, with t denoting the major transpose of a third-order tensor. In this work, the constitutive forms (A1) and (A2)—and also the respective relations between the involved coefficients—hold true for both local behavior of piezoelectric fibers, as well as the corresponding effective behaviors at mesoscale (layers) and macroscale (LPCs).

APPENDIX B: ELECTROSTATIC ESHELBY MATRIX FOR ELLIPTICAL FIBERS AND LAYERS

In this appendix, we express the relevant formulas for the components of the Eshelby matrix S_{IjKl} for the case of cylindrical inclusions with an elliptical cross section, and also for laminated composites. The matrix S_{IjKl} is expressed in terms of surface integrals over the unit sphere. For elliptical geometry of the inclusion, the general components of this matrix may be expressed as

$$S_{IjKl} = \begin{cases} \frac{\alpha}{4\pi} L_{mNKl} \int_0^{2\pi} \frac{[G_{iNmj}(\boldsymbol{\xi}) + G_{jNmi}(\boldsymbol{\xi})]}{\xi_1^2 + \alpha^2\xi_2^2} d\varphi, & I = 1,2,3 \\ \frac{\alpha}{2\pi} L_{mNKl} \int_0^{2\pi} \frac{G_{4Nmj}(\boldsymbol{\xi})}{\xi_1^2 + \alpha^2\xi_2^2} d\varphi, & I = 4 \end{cases}, \tag{B1}$$

where $G_{IJmn}(\boldsymbol{\xi}) = (L_{pIJq}\xi_p\xi_q)^{-1}\xi_m\xi_n$, with $\xi_1 = \cos(\varphi)$, $\xi_2 = \sin(\varphi)$, and $\xi_3 = 0$. The Eshelby matrix $\mathbf{S}^F$ in relation (7) is obtained by specializing relations (B1) to the case of an inactive isotropic matrix for which derivation of closed-form expressions for nonzero components of the Eshelby matrix is feasible. These expressions are available in Appendix A of Ref. [11] and are omitted here for the sake of brevity.

As mentioned in the paper, the laminate geometry is a special case of elliptical geometry where one of the in-plane axes of the elliptical cross section tends to infinity. Here, we define this geometry by the limit $\alpha \to 0$, which corresponds to a laminate with a lamination direction parallel to $\mathbf{e}_2$. The Eshelby tensor $\mathbf{S}^L$ in relation (13) is obtained by replacing L_{mNKl} with $L^{(\mathrm{I})}_{mNKl}$ in expression (B1) and taking the limit of $\alpha \to 0$. It can be shown that the final form of $\mathbf{S}^L$ is expressed as

$$S^L_{IjKl} = \begin{cases} L^{(\mathrm{I})}_{mNKl}[G^{(\mathrm{I})}_{iNmj}(\mathbf{N}) + G^{(\mathrm{I})}_{jNmi}(\mathbf{N})]/2, & I = 1,2,3 \\ L^{(\mathrm{I})}_{mNKl}G^{(\mathrm{I})}_{4Nmj}(\mathbf{N}), & I = 4 \end{cases}, \tag{B2}$$

where $G^{(\mathrm{I})}_{IJmn}(\mathbf{N}) = (L^{(\mathrm{I})}_{pIJq}N_pN_q)^{-1}N_mN_n$, with the unit vector $\mathbf{N} = \mathbf{e}_2$ denoting the lamination direction. Therefore, closed-form expressions for the components S^L_{IjKl} can be derived; however, they are omitted here for the sake of brevity.

[1] H. A. Sodano, G. Park, D. J. Leo, and D. J. Inman, Use of piezoelectric energy harvesting devices for charging batteries, Proc. SPIE Int. Soc. Opt. Eng. **5050**, 101 (2003).

[2] S. R. Anton and H. A. Sodano, A review of power harvesting using piezoelectric materials (2003–2006), Smart Mater. Struct. **16**, R1 (2007).

[3] A. Erturk and D. J. Inman, *Piezoelectric Energy Harvesting* (John Wiley & Sons, New York, 2011).
[4] C. R. Bowen, H. A. Kim, P. M. Weaver, and S. Dunn, Piezoelectric and ferroelectric materials and structures for energy harvesting applications, Energy Environ. Sci. **7**, 25 (2014).
[5] R. E. Newnham, D. P. Skinner, and L. E. Cross, Connectivity and piezoelectric-pyroelectric composites, Mater. Res. Bull. **13**, 525 (1978).
[6] L. V. Gibiansky and S. Torquato, On the use of homogenization theory to design optimal piezocomposites for hydrophone applications, J. Mech. Phys. Solids **45**, 689 (1997).
[7] F. Mohammadi, A. Khan, and R. B. Cass, Power generation from piezoelectric lead zirconate titanate fiber composites, MRS Online Proc. Libr. **736**, D5.5 (2002).
[8] I. Babu and G. de With, Highly flexible piezoelectric 0–3 PZT-PDMS composites with high filler content, Compos. Sci. Technol. **91**, 91 (2014).
[9] H. A. Sodano, D. J. Inman, and G. Park, Comparison of piezoelectric energy harvesting devices for recharging batteries, J. Intell. Mater. Syst. Struct. **16**, 799 (2005).
[10] D. P. Skinner, R. E. Newnham, and L. E. Cross, Flexible composite transducers, Mater. Res. Bull. **13**, 599 (1978).
[11] M. L. Dunn and M. Taya, Micromechanics predictions of the effective electroelastic moduli of piezoelectric composites, Int. J. Solids Struct. **30**, 161 (1993).
[12] R. Hashemi, G. J. Weng, M. H. Kargarnovin, and H. M. Shodja, Piezoelectric composites with periodic multi-coated inhomogeneities, Int. J. Solids Struct. **47**, 2893 (2010).
[13] P. Han, S. Pang, J. Fan, X. Shen, and T. Pan, Highly enhanced piezoelectric properties of PLZT/PVDF composite by tailoring the ceramic Curie temperature, particle size and volume fraction, Sens. Actuators **204**, 74 (2013).
[14] G. W. Milton, Composite materials with Poisson's ratios close to −1, J. Mech. Phys. Solids **40**, 1105 (1992).
[15] E. Galipeau and P. Ponte Castañeda, Giant field-induced strains in magnetoactive elastomer composites, Proc. R. Soc. A **469**, 20130385 (2013).
[16] D. M. Barnett and J. Lothe, Dislocations and line charges in anisotropic piezoelectric insulators, Phys. Status Solidi B **67**, 105 (1975).
[17] J. D. Eshelby, The determination of the elastic field of an ellipsoidal inclusion, and related problems, Proc. R. Soc. A **241**, 376 (1957).
[18] W. F. J. Deeg, Ph.D. thesis, Stanford University, 1980.
[19] M. L. Dunn and M. Taya, An analysis of piezoelectric composite materials containing ellipsoidal inhomogeneities, Proc. R. Soc. A **443**, 265 (1993).
[20] T. Mori and K. Tanaka, Average stress in matrix and average elastic energy of materials with misfitting inclusions, Acta Metall. **21**, 571 (1973).
[21] L. V. Gibiansky and S. Torquato, Matrix laminate composites: Realizable approximations for the effective moduli of piezoelectric dispersions, J. Mater. Res. **14**, 49 (1999).
[22] P Ponte Castañeda and J. R. Willis, The effect of spatial distribution on the effective behavior of composite materials and cracked media, J. Mech. Phys. Solids **43**, 1919 (1995).
[23] H. L. Duan, B. L. Karihaloo, J. Wang, and X. Yi, Effective conductivities of heterogeneous media containing multiple inclusions with various spatial distributions, Phys. Rev. B **73**, 174203 (2006).
[24] G. W. Milton, *The Theory of Composites* (Cambridge University Press, Cambridge, England, 2002).
[25] J. Yu Li and M. L. Dunn, Variational bounds for the effective moduli of heterogeneous piezoelectric solids, Philos. Mag. A **81**, 903 (2001).
[26] P. Bisegna and R. Luciano, Variational bounds for the overall properties of piezoelectric composites, J. Mech. Phys. Solids **44**, 583 (1996).
[27] J. Yang, *An Introduction to the Theory of Piezoelectricity*, Vol. 9 (Springer Science +Business Media, Berlin, 2004).
[28] Y. i. Qi and M. C. McAlpine, Nanotechnology-enabled flexible and biocompatible energy harvesting, Energy Environ. Sci. **3**, 1275 (2010).
[29] S. Priya, Criterion for material selection in design of bulk piezoelectric energy harvesters, IEEE Trans. Ultrason. Ferroelectr. Freq. Control **57**, 2610 (2010).
[30] R. S. Lakes, Piezoelectric composite lattices with high sensitivity, Philos. Mag. Lett. **94**, 37 (2014).
[31] B. Rodriguez, H. Kalathur, and R. S. Lakes, A sensitive piezoelectric composite lattice: Experiment, Phys. Status Solidi B **251**, 349 (2014).
[32] R. Hashemi, Magneto-electro-elastic properties of multiferroic composites containing periodic distribution of general multi-coated inhomogeneities, Int. J. Eng. Sci. **103**, 59 (2016).